J. Fluid Mech. (1983), *vol.* 136, *pp.* 111–137
Printed in Great Britain

Turbulent dispersion from an elevated line source: measurements of wind-concentration moments and budgets

By M. R. RAUPACH
CSIRO Division of Environmental Mechanics, GPO Box 821, Canberra, ACT 2601, Australia
AND B. J. LEGG
Rothamsted Experimental Station, Harpenden, Herts, U.K.

(Received 1 March 1983)

Wind and tracer-concentration fluctuations, and hence the budgets for tracer variance, vertical flux and streamwise flux, have been measured in the dispersing plume from an elevated lateral line source in an equilibrium turbulent surface layer, using heat as a passive tracer. The results are analysed by testing closure assumptions for models of turbulent dispersion at first and second order. Except close to the source, a first-order (gradient-diffusion) model satisfactorily predicts both the vertical and streamwise tracer fluxes.

The tracer-variance budget is essentially a balance between advection and dissipation, with production becoming significant as fetch increases. The vertical and streamwise heat-flux budgets have advection and turbulent-transport terms which are in balance (almost exactly for the vertical flux, only approximately for the streamwise flux), leaving balances between local production and pressure-gradient interaction. The turbulence-interaction component of the pressure term cannot be modelled as $-\overline{u_i'\theta'}/\tau$, $\overline{u_i'\theta'}$ being the flux vector and τ a scalar timescale.

1. Introduction

The dispersion of a passive tracer from an elevated source in a turbulent boundary layer is worthy of study for several reasons. From the practical viewpoint, it is an important transport problem in environmental meteorology, relevant to the dispersion of pollutants, pollen, plant disease spores, spray droplets and so on. More fundamentally, it poses a challenge for theoretical models which aim to predict the dispersion of a passive tracer released into an arbitrary turbulent flow, given sufficient information about the flow velocity statistics. These models are of several kinds, including simple gradient-diffusion models, with well-known limitations (Corrsin 1974); higher-order closure models, which require careful selection and testing of the necessary closure assumptions (e.g. Launder 1976); Lagrangian-statistical theories, which use similarity concepts to determine Lagrangian flow properties and which are therefore limited to self-preserving flows (Batchelor 1957; Hunt & Weber 1979); and Markov-chain simulations of fluid-particle trajectories, which require prior knowledge of, or assumptions about, Lagrangian velocity statistics (e.g. Legg 1983).

Most laboratory experiments on dispersion from line or point sources in turbulent boundary layers have examined the mean tracer concentration field only, a typical line-source experiment being that of Shlien & Corrsin (1976), who also review earlier work. The fluctuating concentration field has been studied far less. Belorgey, Nguyen

& Trinite (1980) measured both the mean and fluctuating temperature fields from elevated line heat sources over smooth walls with differing boundary conditions for heat; both perfectly insulating (zero heat flux) and perfectly conducting (constant-temperature) walls were used. Recently, during the course of this work, Fackrell & Robins (1981, 1982) published an extensive study on concentration fluctuations and fluxes in plumes from elevated and ground-level point sources in a turbulent boundary layer; this followed their earlier work (Robins & Fackrell 1979) in which fluxes were not measured directly.

The purpose of this paper is to present the results of an experiment on passive tracer dispersion from an elevated line source in a turbulent boundary layer, with emphasis on the temperature fluctuation field and the wind-temperature covariances. The results are used to test some assumptions currently used in higher-order closure models for predicting dispersion. Wherever possible, the results will be compared with those of Fackrell & Robins, given principally in their 1982 paper (denoted as FR).

The experiment described here is the first of a series on the turbulent dispersion of a passive tracer, the eventual application being to turbulent dispersion (of CO_2, water vapour, pollen, spores, etc.) in vegetation canopies. Other experiments will study a plane source on a rough wall, and line and plane sources within a model plant canopy.

2. Experimental details

2.1. *Wind tunnel and heat source*

The experiment was done in the CSIRO Pye Laboratory wind tunnel, an open-return, blower tunnel with a 5.5:1 two-dimensional contraction and a working section 10.6 m long, 1.8 m wide and 0.7 m high (Wooding 1968). The tunnel was designed to simulate the flow in the adiabatic atmospheric surface layer. The configuration and axes are shown in figure 1. A 50 mm fence tripped the flow entering the working section, generating a deep turbulent boundary layer which was allowed to equilibrate over a rough surface made by gluing road gravel (nominal diameter 7 mm) to wooden baseboards of thickness 12 mm. The baseboards were placed in the tunnel over a sheet of polystyrene foam (25 mm thick) to give good thermal insulation. The flexible roof of the working section was adjusted to give zero static pressure gradient, to within 1 % of the freestream dynamic pressure, over the working range.

The line heat source was a 0.9 mm diameter nichrome wire, tensioned laterally across the tunnel at a height of 60 mm above the zero-plane of the surface. Welded brass tubes fixed the active, heated length of wire at 1.60 m (0.2 m less than the tunnel width). The wire was heated electrically with an a.c. supply (21A, 55 V at maximum) which gave a steady power to within 1 %.

2.2. *Wind and temperature sensors*

The streamwise (u) and vertical (w) velocity components were measured with a constant-temperature X-wire anemometer (DISA probe type P61) using platinum wires of diameter 5 μm and length 1 mm, run at an overheat ratio of 2.0 by hot-wire bridges (Thermo-Systems Inc., 1050 series). To account for the presence of temperature fluctuations, a small correction (less than 3 % of wind speeds) was applied to the hot-wire signals. This was based on the heat-transfer law of Collis & Williams (1959) for a long hot wire exposed normally to an air flow at low Reynolds number ($0.02 < Re < 44$):

$$Nu\left(\frac{T_w+T}{2T}\right)^{-0.17} = 0.24+0.56Re^{0.45},$$

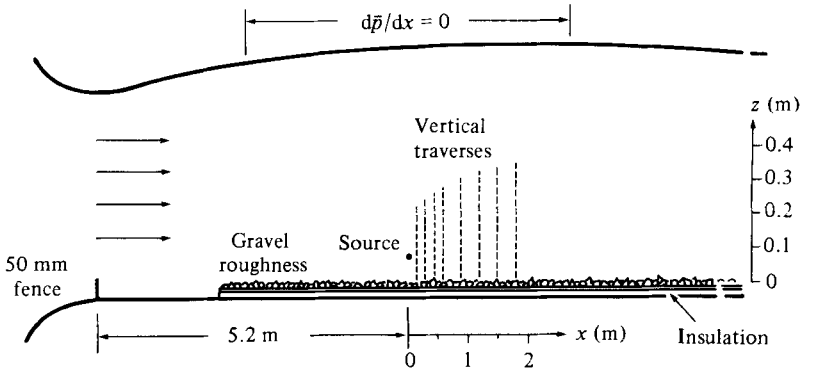

FIGURE 1. The experimental configuration in the wind tunnel. Note expanded vertical scale.

where Nu is the Nusselt number, T the air temperature and T_w the wire temperature. Using the fact that the heat loss from the wire is proportional to E^2/R (where E is the output of the constant-temperature hot-wire bridge and R the wire resistance), it follows that, to first order,

$$\frac{E_c}{E} = 1+\frac{1}{2}\left(1+\frac{0.17T_w(T_w-T_a)}{(T_w+T_a)T_a}\right)\frac{\theta}{T_w-T_a}, \tag{1}$$

where E is the measured anemometer output, E_c the output after correction for temperature fluctuations, T_a the mean ambient temperature of the air and θ the air temperature relative to T_a (so that $\theta = T-T_a$).

The temperature θ was measured with a cold-wire resistance thermometer (90 % Pt, 10 % Rh) of typical length 1.5 mm and of diameter 1.2 μm (for most runs) or 0.63 μm (for temperature-dissipation measurement; see below). The cold wire was supplied with a current of 162 μA from a Wheatstone bridge circuit, after which the θ-signal was amplified by 10^4 with a specially designed low-noise amplifier. The resolution (smallest measurable mean temperature difference) of the thermometer was 0.005 K, the r.m.s. noise 0.03 K and the half-power frequency 1.5 kHz for a 1.2 μm cold wire and 5 kHz for a 0.63 μm wire, at a wind speed of 8 m s^{-1}. (The frequency response was measured by superimposing on the d.c. bridge head voltage a square wave of sufficient amplitude to raise the wire temperature by 1 K.) The sensitivity of the thermometer to wind fluctuations was less than 0.005 K per m s^{-1}, a negligible value.

2.3. *Acquisition, analysis and scaling of data*

The wind and temperature sensors were mounted on a traversing mechanism, with the cold wire vertically oriented and displaced laterally from the X-wire by 2 mm. To eliminate slow drifts in the ambient temperature and thermometer circuitry, the procedure at each measurement point was to record the background temperature with the heat source off, turn the source on, wait 40 s (sufficient for equilibrium) and then record all signals. Several 20-point vertical profiles were measured in this way at each of eight streamwise stations from $x = 0.15$ m to $x = 1.8$ m.

The source power was always small enough to regard the heat as a passive additive (the ratio of buoyancy to inertial forces was 2.3×10^{-4} at maximum). To keep the temperature signal within range and to minimize the X-wire temperature correction, the source power was decreased for runs at small x (it varied by a factor of 10 through

the experiment). A small radiation loss from the source, at most 11 % of the source power, was calculated from the source temperature (estimated from the source resistance) using the Stefan–Boltzmann equation.

The signals were low-pass filtered at 0.8 kHz (Butterworth, 96 db/octave), digitized on-line at 2 kHz, and recorded on magnetic tape continuously for 20 s at each measurement position. Subsequent digital processing produced time series and moments for u, w and θ by (*a*) applying a linear temperature calibration for θ; (*b*) using (1) to remove temperature contamination from the X-wire voltages; (*c*) applying a nonlinear wind calibration to obtain effective X-wire cooling velocities; (*d*) solving for u and w, taking account of the axial cooling effect (Champagne, Sleicher & Wehrmann 1967) but ignoring the lateral velocity component v.

To obtain vertical and streamwise gradients of moments of u, w and θ, a cubic spline (program SMOOTH; de Boor 1978) was fitted to each individual vertical profile of each moment, after normalizing θ (see below). The resulting fitted values and z-derivatives, read at 35 preset heights from 5 to 250 mm, were averaged over all replicate profiles at each streamwise station. To determine x-derivatives, a second cubic spline was fitted against x at each height, for each moment.

Most results will be presented in dimensionless form, using the source height h as a lengthscale and the friction velocity u_* as a velocity scale (u_* is the value of $(-\overline{u'w'})^{\frac{1}{2}}$ in the constant-stress region, overbars denoting time averages and primes departures therefrom). A temperature scale θ_* is defined by

$$\theta_* = \frac{Q}{\rho c_p h \bar{u}(h)}, \tag{2}$$

where Q is the line source strength or power per unit length, ρ the air density and c_p the specific heat of air at constant pressure. The choice of h as a lengthscale and u_* as a velocity scale is consistent with surface-layer similarity theory, and hence is appropriate when the plume is principally in the surface layer, as in this experiment. (In contrast, FR used the boundary-layer depth δ as their lengthscale.) The temperature scale θ_* has the property that, when the plume depth is of order h, $\bar{\theta}/\theta_*$ is of order 1. The practical evaluation of Q is considered in §3.1.

2.4. *The wind field*

Figure 2 shows mean wind profiles at $x = 0.15$ m and $x = 1.8$ m, plotted against $\ln z$. The zero-plane $z = 0$ was set 6 mm above the substrate surface underlying the gravel roughness; this choice gave the best fit of the mean wind profile to the logarithmic law

$$\bar{u}(z) = \frac{u_*}{k} \ln \frac{z}{z_0}, \tag{3}$$

where k is the von Kármán constant and z_0 the roughness length. From the measured $\overline{u'w'}$ profiles (figure 3), u_* was 0.48 m s^{-1} in the middle of the experimental range of x, varying by less than ± 3 %; this gave fitted values $k = 0.38$ and $z_0 = 0.12$ mm. The value for k is well within the accepted range.

The profiles of $\overline{u'w'}$, and of the standard deviations $\sigma_u = (\overline{u'^2})^{\frac{1}{2}}$ and $\sigma_w = (\overline{w'^2})^{\frac{1}{2}}$, are similar to observations in fully developed rough-wall turbulent boundary layers with zero pressure gradient (e.g. Raupach 1981). There was a slight decrease (≈ 10 %) in turbulence intensity over the range $x = 0.15$ m to 1.8 m; this was sufficiently small that, from the point of view of this experiment, the boundary layer was in streamwise equilibrium. The slight decay in $|\overline{u'w'}|$ as $z \to 0$ is a common feature of rough-wall

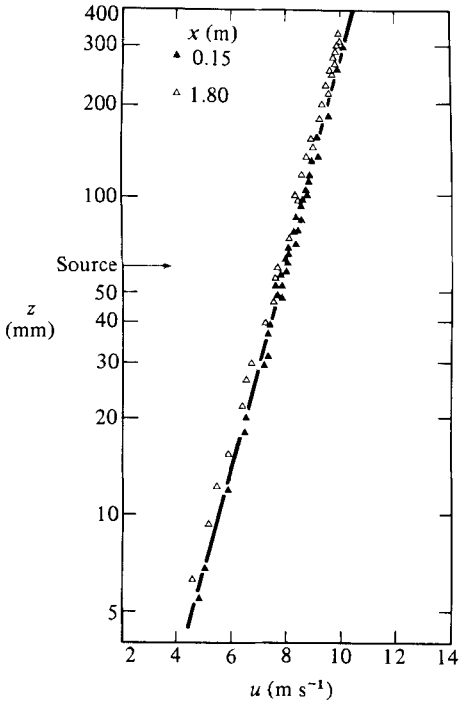

FIGURE 2. Profiles of $\bar{u}$ against $\ln z$.

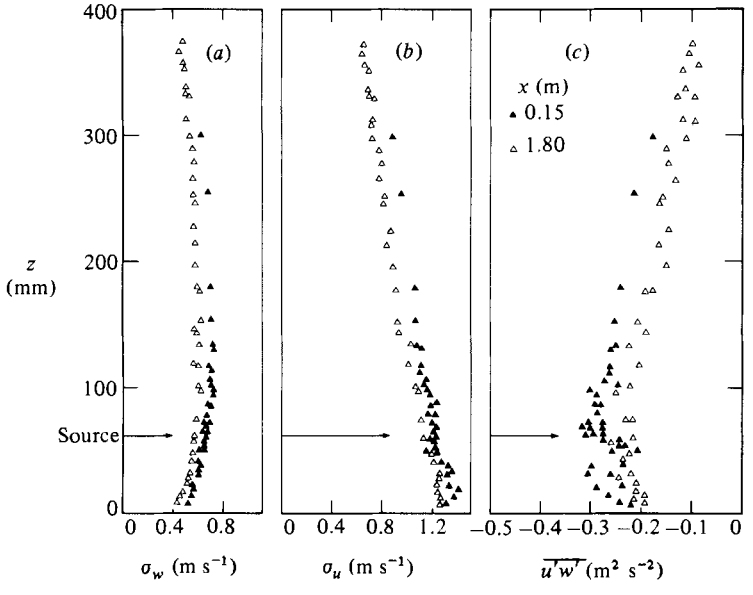

FIGURE 3. Profiles of wind statistics: (*a*) σ_w; (*b*) σ_u; (*c*) $\overline{u'w'}$.

turbulent-boundary-layer observations in wind tunnels (Mulhearn & Finnigan 1978), but it can be fully explained by the known limitations of X-wires in the high-intensity turbulence near the wall (Raupach, Thom & Edwards 1980). It is thus unlikely to be real.

Source height	h	(mm)	60
Boundary-layer depth	δ	(mm)	540
Mean wind speeds	$\overline{u}(h)$	(m s^{-1})	7.8
	$\overline{u}(\delta)$	(m s^{-1})	11.0
Friction velocity	u_*	(m s^{-1})	0.48
Roughness length	z_0	(mm)	0.12
Reynolds numbers:			
boundary-layer	$\overline{u}(\delta)\,\delta/\nu$		4×10^5
roughness	$u_* z_0/\nu$		3.8

TABLE 1. Summary of basic flow parameters

z (mm)	z/h	z/δ	η (mm)	η_θ/l_w	$\sigma_w/(-\overline{u'w'})^{\frac{1}{2}}$	$\sigma_u/(-\overline{u'w'})^{\frac{1}{2}}$
30	0.5	0.06	0.14	0.23	1.15	2.48
60	1	0.11	0.17	0.27	1.29	2.30
120	2	0.22	0.20	0.32	1.43	2.15
180	3	0.33	0.22	0.36	1.48	2.06

TABLE 2. Height-dependent flow parameters at $x = 0.90$ m

Because a tripping fence was used to generate a deep floor boundary layer, there was no completely non-turbulent freestream between the floor and roof boundary layers. As a substitute for the boundary-layer depth δ, we use the height of the maximum in $\overline{u}$, which was 0.54 m over the working range of x (cf. the tunnel height of 0.7 m). At $z = \delta$, the flow was predominantly non-turbulent (the intermittency was about 0.1). The absence of a classical outer layer, capped by a non-turbulent flow, is not a serious weakness in this experiment because the heated plume was confined to the region $z \lesssim 0.3$ m.

Tables 1 and 2 summarize the main aerodynamic parameters, taking $x = 0.90$ m as a representative station. For later comparisons, we note the following dimensionless ratios for our experiment, with values for FR's experiment in parentheses:

$$h/\delta = 0.11 \qquad (0.19);$$

$$u_*/\overline{u}(\delta) = 0.044 \qquad (0.047);$$

$$z_0/\delta = 2.2 \times 10^{-4}\ (2.4 \times 10^{-4}).$$

Hence the boundary layers are essentially identical, the only difference (apart from FR's use of a point source) being in h/δ.

2.5. *Dissipation rate for temperature fluctuations*

The dissipation rate ϵ_θ for temperature fluctuations ($\frac{1}{2}\overline{\theta'^2}$) was measured separately from the main experiment. Assuming local isotropy and Taylor's hypothesis, we have

$$\epsilon_\theta = \kappa\left(\overline{\left(\frac{\partial\theta'}{\partial x}\right)^2} + \overline{\left(\frac{\partial\theta'}{\partial y}\right)^2} + \overline{\left(\frac{\partial\theta'}{\partial z}\right)^2}\right) \approx \frac{3\kappa}{\overline{u}^2}\overline{\left(\frac{\partial\theta'}{\partial t}\right)^2}, \tag{4}$$

where κ is the thermal diffusivity of air and t time. The temperature signal from a cold wire (length 0.8 mm, diameter 0.63 μm) was low-pass filtered at 20 kHz, differentiated with an analogue differentiator with unit gain at 217 Hz and linear

response to 5 kHz, and finally squared and averaged by analog methods, thus giving a measured value V for the variance of $\partial\theta'/\partial t$. The effect of electrical noise was removed by measuring V with the heat source both on and off and using the difference $V_{on}-V_{off}$ to calculate ϵ_θ from (4); this procedure assumes that the $\partial\theta'/\partial t$ signal is independent of the noise. Measurements of ϵ_θ were made at $x = 0.45$, 0.90 and 1.50 m; at these stations, the signal-to-noise ratios $(V_{on}-V_{off})/V_{off}$ at the heights of maximum ϵ_θ (see figure 12) were 50, 7 and less than 1 respectively. The measurements at $x = 1.50$ m were discarded because of the poor signal-to-noise ratio.

Apart from noise, the principal errors in measuring $\overline{(\partial\theta'/\partial t)^2}$ are caused by high-frequency losses associated with the finite wire length and the electronics. The loss due to finite wire length depends on the ratio η_θ/l_w, where $\eta_\theta = (\kappa/\nu)^{\frac{3}{4}}\eta = 1.28\eta$ is the Corrsin–Obukhov scale, l_w the wire length, η the Kolmogorov lengthscale and ν the kinematic viscosity. Values of η and η_θ/l_w are given in table 2; our values of η_θ/l_w are similar to those of Sreenivasan, Antonia & Danh (1977), who concluded that the underestimate in $\overline{(\partial\theta'/\partial t)^2}$ due to finite wire length was 15% at most. The electronic high-frequency loss was shown to be small by considering the dimensionless dissipation rate $\hat{\epsilon}_\theta = h\epsilon_\theta/u_*\theta_*^2$, which is independent of wind speed provided the flow (and hence the θ-field) is independent of Reynolds number. This was true for our flow. Since increasing $\bar{u}$ shifts the $\partial\theta'/\partial t$ spectrum to higher frequencies by Taylor's hypothesis, electronic high-frequency loss will appear as a decrease in the measured value of $\hat{\epsilon}_\theta$ with increasing $\bar{u}$. No such decrease was observed until $\bar{u}$ exceeded (by 20%) its working value throughout this experiment; hence electronic high-frequency loss was small.

3. The temperature field

3.1. *Heat conservation*

The conservation equation for mean temperature is, for steady, laterally homogeneous conditions,

$$\bar{u}\frac{\partial\bar{\theta}}{\partial x}+\frac{\partial}{\partial x}\overline{u'\theta'}+\frac{\partial}{\partial z}\overline{w'\theta'} = q(x,z), \tag{5}$$

where $q(x,z)$ is a source strength function, given in our case by $q_s\delta(0,h)$, $\delta(x,z)$ being the two-dimensional Dirac delta function. Molecular transport is assumed negligible. Integrating over z from 0 to ∞ and over x from $-\infty$ to the station of interest, and assuming $\overline{w'\theta'} = 0$ at $z = 0$ and $\theta\to 0$ as $z\to\infty$, we obtain (for $x > 0$) the integral conservation equation

$$Q_I(x) = \rho c_p\int_0^\infty(\bar{u}\bar{\theta}+\overline{u'\theta'})\,dz = Q_S = \rho\, c_p q_s, \tag{6}$$

where Q_S is the line source strength in W m^{-1}, given in our case by the electrical power less radiation loss, and $Q_I(x)$ is the total streamwise heat flux through a vertical plane at x, defined by (6). Values of Q_I, calculated for each run by integrating $\bar{u}\bar{\theta}+\overline{u'\theta'}$ from the ground to the maximum height of measurement (typically 330 mm), are compared with Q_S values in figure 4 by plotting Q_I/Q_S against x/h. This ratio was close to unity for $x/h \leqslant 10$, but declined thereafter, with increasing x, to about 0.8 at $x/h = 30$, implying a heat loss of 20% at that distance. The measured turbulent heat fluxes $\overline{w'\theta'}$ to the wind-tunnel floor and from the top of the plume were small, accounting for less than a quarter of the observed loss (see figure 6). Radiation losses from the plume itself, as distinct from the source, were insignificant. Most of the

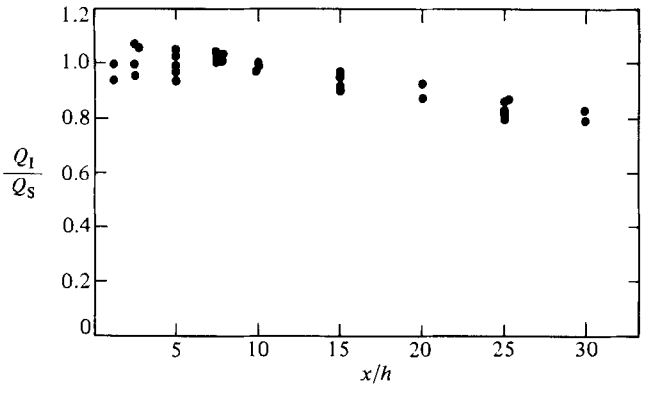

FIGURE 4. The ratio Q_I/Q_S.

apparent heat loss was probably caused by lateral transport associated with the downstream broadening of the plume from the source wire length of 1.60 m to the full tunnel width of 1.80 m, and with the subsequent heat loss through the sidewalls of the tunnel. The situation is complicated by the three-dimensionality of the mean flow within about 0.3 m of the sidewalls, due to sidewall boundary layers.

The changes in source power through the experiment (see §2.3) were scaled out using (2), with $Q = Q_I$. The use of Q_I in (2) removes from θ/θ_* the apparent advective effects introduced by the heat loss shown in figure 4, at least to a first approximation. An alternative procedure would be to scale θ with Q_S instead of Q_I; this would make no significant difference to the results and conclusions which follow, except for small changes ($\lesssim 10\%$) in the relative magnitudes of the advection terms in the budgets of $\bar{\theta}$, $\overline{\theta'^2}$, $\overline{w'\theta'}$ and $\overline{u'\theta'}$.

3.2. *Mean and fluctuating temperatures*

Mean-temperature profiles are shown in figure 5(*a*) at four representative values of x/h. The mean plume is fairly symmetrical at $x/h = 2.5$, but becomes progressively more positively skewed with increasing x as downward dispersion is limited by the ground. At the largest fetch, $x/h = 30$, $\bar{\theta}/\theta_*$ is approximately uniform for $z/h < 0.6$; hence the available fetch is insufficient to permit the plume to reach the stage at which it resembles the plume from a ground-level source. Such a plume would have a $\bar{\theta}$-profile proportional to $\exp(-z^s)$, $s \approx 1.3$ (Sutton 1953). The ground-level mean temperature $\bar{\theta}_0$ (figure 5*a*, inset) is at a maximum at about $x/h = 21$.

These results are strikingly similar to the results of FR for the mean centreline concentrations from their elevated point source, provided that x and z are normalized with h rather than δ. Table 3 compares the positions of maximum $\bar{\theta}_0$ and the points of contact of the plumes with the ground (defined here as the upstream x-value at which $\bar{\theta}_0$ is 10% of maximum) from our experiment (RL) and from FR. The close agreement in values of x/h confirms that surface-layer scaling (that is, scaling of lengths with h) successfully accounts for variations in h/δ, at least up to about 0.2. However, we must note that a strict similarity comparison should have used laterally integrated θ-values from the point source rather than centreline values; we have assumed that the two produce the same points of contact and ground-level maxima. Also, we have relied upon the (accidental) fact that the two boundary layers are nearly identical (§2.4). Clearly, this type of similarity could not otherwise be observed.

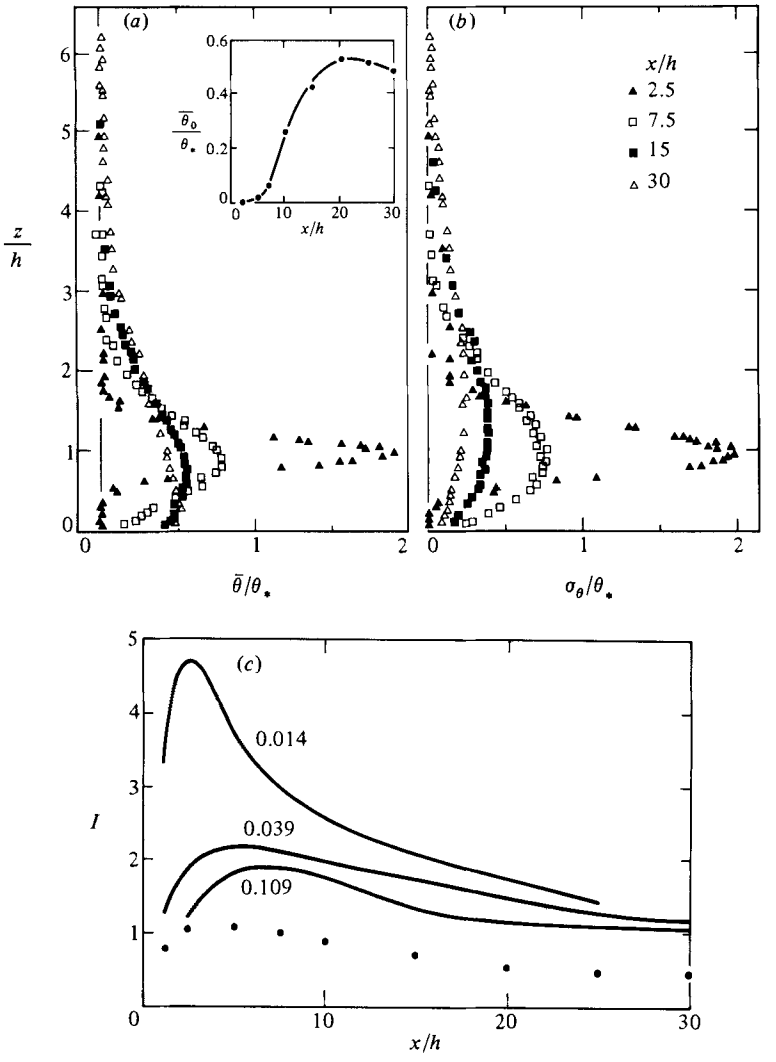

FIGURE 5. (*a*) Mean-temperature profiles; inset shows variation with x of mean ground temperature $\bar{\theta}_0$. (*b*) Profiles of standard deviation of temperature. (*c*) Relative intensity $I(x) = \sigma_{\theta\max}/\theta_{\max}$ for elevated line source with $d/h = 0.015$ (points), and for 3 elevated point sources with values of d/h as shown (lines; data from FR).

	Maximum in $\bar{\theta}_0$		Point of contact	
	RL	FR	RL	FR
x/h	21	17	7.5	8
x/δ	2.4	3.3	0.83	1.6

TABLE 3. Values of x/h and x/δ at maximum in $\bar{\theta}_0$ and at point of contact of plume with ground

Profiles of the standard deviation of θ, $\sigma_\theta = (\overline{\theta'^2})^{\frac{1}{2}}$, are shown in figure 5(*b*). These are similar to the $\bar{\theta}$-profiles except that they are broader because of the high intermittency of the θ-signal near the free edges of the plume. Also, σ_θ diminishes as the surface is approached far more rapidly than does $\bar{\theta}$, because of the tendency of the advection and production terms in the $\frac{1}{2}\overline{\theta'^2}$ budget (the main terms increasing $\frac{1}{2}\overline{\theta'^2}$) to approach zero as $z \to 0$. (The $\frac{1}{2}\overline{\theta'^2}$ budget is discussed in §5.1.) Qualitatively similar results were obtained by FR for the centreline behaviour of σ_θ from an elevated point source. There, as here, it appears that σ_θ approaches, but does not reach, zero at the ground, although neither experiment is unequivocal.

The σ_θ field from an elevated source is strongly dependent on source size, but the $\bar{\theta}$ field is not, essentially because σ_θ is controlled by the meandering of a narrow instantaneous plume that broadens only slowly with x, whereas $\bar{\theta}$ is largely independent of the instantaneous plume width. FR demonstrated the effect of source size on σ_θ by considering the relative intensity $I = \sigma_{\theta\max}/\bar{\theta}_{\max}$, where the subscript denotes the maximum value found at any given x. They presented $I(x)$ for elevated point sources of several different diameters d. Their results are compared with ours (for a single elevated line source with $d/h = 0.015$) in figure 5(*c*). Clearly, the change from a point to a line source with similar d/h has a very large effect on I, reducing it by a factor between 2 and 5, depending on x/h. A qualitative explanation is that only vertical meandering of the instantaneous line source plume causes intermittency in θ, whereas both vertical and lateral meandering contribute for the point source plume. Detailed θ-statistics for the present data (intermittencies, probability-density functions, moments) will be presented in another paper.

3.3. *Vertical and streamwise heat fluxes*

Figure 6(*a*) shows $\overline{w'\theta'}$ at $x/h = 7.5$, while the curves in figure 6(*b*) are fits to the measurements of $\overline{w'\theta'}$ at $x/h = 2.5$, 7.5, 15 and 30. In this way, both the quality of the data and the streamwise evolution of $\overline{w'\theta'}$ are indicated. The $\overline{w'\theta'}$ profile near the source is skew-symmetric about the height at which $\bar{\theta}$ is maximum, the heat flux being everywhere directed away from this height. With increasing x, the profile distorts from skew-symmetry until it becomes bow-shaped and everywhere positive. Again, the profile closely resembles FR's centreline data for an elevated point source, the agreement being excellent under surface-layer scaling; for example, $\overline{w'\theta'}$ becomes positive-definite with height at about $x/h = 25$ in both cases.

Figure 7 shows profiles of $\overline{u'\theta'}$, which evolve with x/h in a way similar to the $\overline{w'\theta'}$ profiles except that $\overline{u'\theta'}$ and $\overline{w'\theta'}$ are almost everywhere opposite in sign. The magnitude of $|\overline{u'\theta'}/\overline{w'\theta'}|$ is as high as 6 near the ground, but falls to 1 or less in the upper part of the plume. The assumption $\overline{u'\theta'}/\overline{w'\theta'} \approx -3$ (Monin & Yaglom 1971, p. 522), often used in adiabatic surface layers for heat or tracer released from a large area source near the ground, does not apply here. FR did not present measurements of $\overline{u'\theta'}$.

An important consistency check is provided by calculating the terms in the mean-temperature conservation equation (5). Figure 8 shows profiles of terms in this budget for $x/h = 7.5$, 15 and 25 (the streamwise gradient calculation was unreliable outside this range). The budget is essentially a balance between streamwise advection of $\bar{\theta}$ and vertical divergence of $\overline{w'\theta'}$. The residual term (the measured value of the left-hand side of (5)) is typically 10–20% of the dominant terms in the budget, and shows no clear sign preference, except at $x/h = 25$, where $-\bar{u}\,\partial\bar{\theta}/\partial x$ is underestimated because of the measurement difficulties caused by weak streamwise $\bar{\theta}$-gradients. This result suggests that our analysis procedure is capable of closing budgets to within

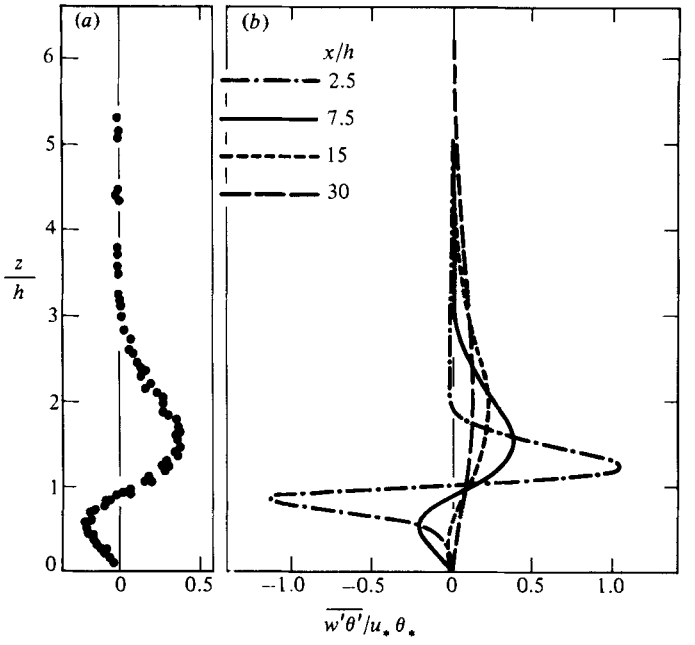

FIGURE 6. (*a*) Measured values of $\overline{w'\theta'}$ at $x/h = 7.5$. (*b*) Fitted $\overline{w'\theta'}$ profiles.

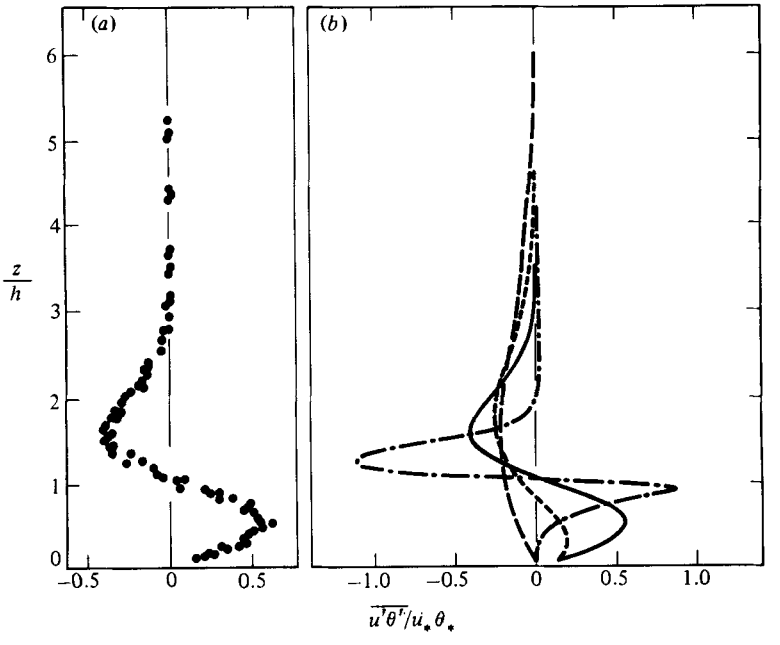

FIGURE 7. (*a*) Measured values of $\overline{u'\theta'}$ at $x/h = 7.5$. (*b*) Fitted $\overline{u'\theta'}$ profiles, with symbols as in figure 6(*b*).

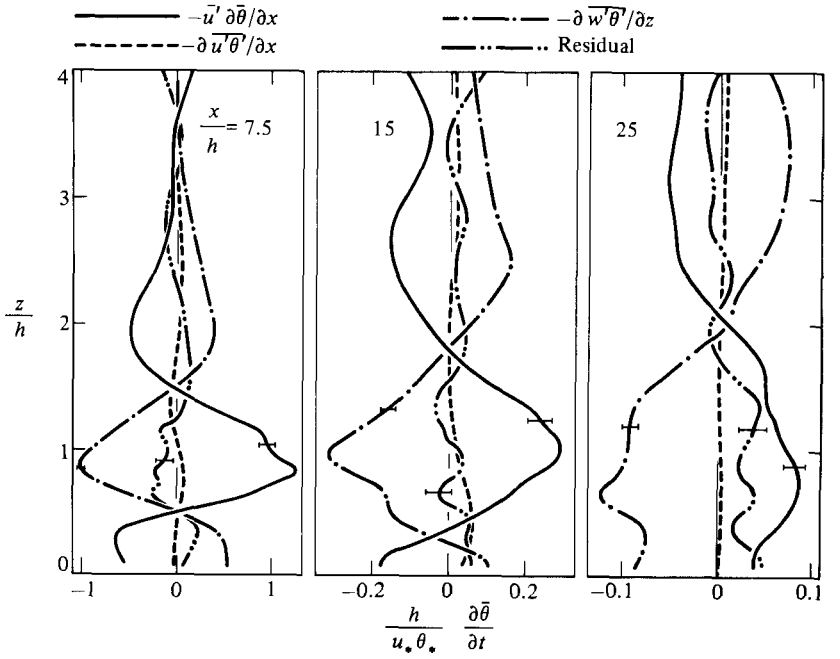

FIGURE 8. Terms in the budget of $\bar{\theta}$, (5). Error bars indicate estimated r.m.s. errors for each term (not shown where negligible).

20 % or better, except possibly far downstream when advection terms are dominant. It also confirms the consistency of the $\overline{w'\theta'}$ measurements.

4. Tests of first-order closure

4.1. *Gradient-diffusion postulate and timescales*

The concurrence between $\overline{w'\theta'}$ and $\partial\bar{\theta}/\partial z$ suggests that the flow might approximately obey the gradient-diffusion postulate

$$\overline{u_i'\theta'} = -K_{ij}\frac{\partial\bar{\theta}}{\partial x_j}, \tag{7}$$

where K_{ij} is the diffusivity tensor $(i,j = 1,2,3)$, $x_i = (x,y,z)$, $u_i = (u,v,w)$, and repeated indices are summed.

An expression for K_{ij} is

$$K_{\alpha\beta} = \overline{u_\alpha' u_\beta'} T_{\alpha\beta}, \tag{8}$$

where there is no summation over Greek indices $(\alpha,\beta = 1,2,3)$, and where $T_{\alpha\beta}$ is a timescale which we expect to be related to the $u_\alpha u_\beta$ integral lengthscale or spectral peak wavelength. (This expectation does not hold near the source; see below.) Note that (8) is not an invariant model (one independent of the choice of axes) unless $T_{\alpha\beta}$ is a scalar, that is, $T_{\alpha\beta}$ takes the same value for all α and β.

To specify $T_{\alpha\beta}$, we use two well-defined timescales. The first, determined by the local velocity field and often used in higher-order-closure models (e.g. Launder 1976; Lumley 1978), is

$$\tau_\epsilon = \frac{c_\epsilon \overline{q^2}}{2\epsilon}, \tag{9}$$

where $\overline{q^2}$ ($= \overline{u'^2}+\overline{v'^2}+\overline{w'^2}$) is twice the turbulent kinetic energy, ϵ the dissipation rate for $\frac{1}{2}\overline{q^2}$ and c_ϵ a constant of proportionality. The approximation $\overline{v'^2} = \frac{1}{2}(\overline{u'^2}+\overline{w'^2})$, which was good to within 5%, was used to compute $\overline{q^2}$ from X-wire data for u and w. In the absence of direct measurements, ϵ was estimated as $0.9u_*^3/kz$, which was valid to within 5% for $0 < z/h < 4$. (Direct measurements of ϵ, and a $\frac{1}{2}\overline{q'^2}$ budget, were obtained during a companion experiment to the present one. The coefficient 0.9 is slightly less than the local-equilibrium value of unity because of the $\frac{1}{2}\overline{q^2}$ loss by turbulent transport in the lower part of the profile ($z/h \lesssim 2$), and a slight overestimate of the local $\frac{1}{2}\overline{q^2}$ production rate ($-\overline{u'w'}\,\partial\bar{u}/\partial z$) by u_*^3/kz in the upper part of the profile.) The final expression used to evaluate τ_ϵ is

$$\tau_\epsilon = \tfrac{3}{4}c_\epsilon(\overline{u'^2}+\overline{w'^2})\frac{kz}{0.9u_*^3}. \tag{10}$$

We fix c_ϵ so that vertical transport obeys (7) with $K_{33} = \overline{w'^2}\tau_\epsilon$; hence $T_{33} = \tau_\epsilon$. This implies that, in the surface layer,

$$K_{33} = \overline{w'^2}\tau_\epsilon = \frac{K_{\mathrm{M}}}{Pr} = \frac{ku_*z}{Pr}, \tag{11}$$

where K_{M} is the vertical turbulent diffusivity for momentum and Pr is the turbulent Prandtl number K_{M}/K_{33}. From (10) and (11),

$$c_\epsilon = \frac{0.9\times\frac{4}{3}}{Pr}\frac{u_*^4}{\overline{w'^2}(\overline{u'^2}+\overline{w'^2})} = 0.09, \tag{12}$$

where the number 0.09 follows from data in table 2 and the value $Pr = 1$ (see later). Note from (11) that, in the surface layer where $\overline{w'^2}/u_*^2$ is (approximately) constant, τ_ϵ is proportional to z/u_*, in accordance with surface-layer similarity theory.

Although τ_ϵ specifies T_{33}, it is not reasonable to use τ_ϵ for other $T_{\alpha\beta}$ components, especially T_{11} and T_{13}. Much experimental evidence shows that timescales associated with streamwise turbulent motions are controlled by outer-layer parameters even in the surface layer. For example, horizontal velocity spectra in the unstable atmospheric surface layer have peak wavelengths that scale with the mixed-layer depth (Kaimal 1978). For a laboratory turbulent boundary layer, Raupach (1981) found that the interval between passages past a fixed point of successive stress-transporting structures, as measured by strong ejection events, scaled with δ/u_* over a wide range of surface roughness. To allow for this type of scaling, we define a second timescale as

$$\tau_\delta = c_\delta\delta/u_*. \tag{13}$$

The constant c_δ is fixed by letting $T_{11} = \tau_\delta$ in (8) and following Corrsin (1974) in taking $K_{11} = 4.5K_{33}$ at $z/\delta = 0.45$. These assumptions give $c_\delta = 0.23$.

4.2. *Gradient-diffusion representations for* $\overline{w'\theta'}$

In two dimensions, (7) and (8) imply for $\overline{w'\theta'}$

$$\underset{\mathrm{I}}{\overline{w'\theta'}} = \underset{\mathrm{II}}{-\overline{w'^2}T_{33}\frac{\partial\bar{\theta}}{\partial z}} \underset{\mathrm{III}}{-\overline{u'w'}T_{31}\frac{\partial\bar{\theta}}{\partial x}}. \tag{14}$$

In figure 9, terms I, II and III of (14) are plotted at $x/h = 2.5$, 7.5, 15 and 25, with T_{33} and T_{31} both set to τ_ϵ. Given the limitations of the gradient-diffusion hypothesis, term III is negligible. Term II is an acceptable representation of $\overline{w'\theta'}$ for $x/h \geqslant 15$, but overestimates $\overline{w'\theta'}$ at smaller x/h.

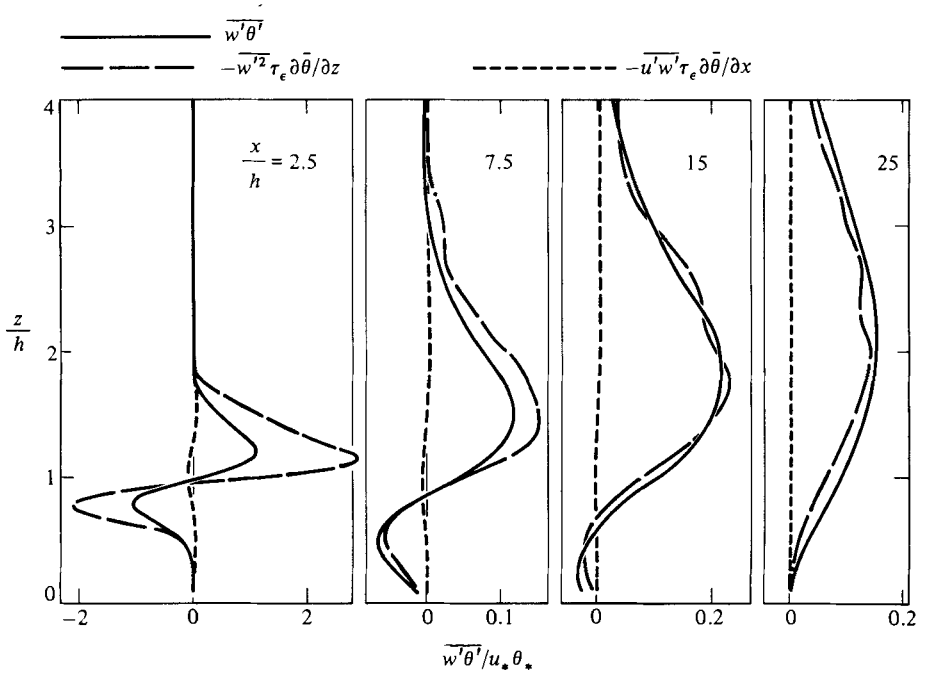

FIGURE 9. Terms in the first-order $\overline{w'\theta'}$ closure, (14).

This result is consistent with the well-known failure of gradient-diffusion theory close to a source in a turbulent flow. Batchelor (1949) showed that dispersion from an instantaneous point source in homogeneous turbulence can be described by a time-dependent effective turbulent diffusivity

$$\hat{K}(t) = \overline{w_L'^2} \int_0^t r_L(\tau)\, d\tau, \tag{15}$$

w_L being the Lagrangian velocity in the direction of dispersion and $r_L(t)$ the autocorrelation function for w_L. If T_L is the integral timescale for r_L, then the large-time limit of $\hat{K}(t)$ is $\overline{w_L'^2}\, T_L$. For our continuous elevated source, an approximate effective diffusivity $\hat{K}_{33}$ can be obtained by neglecting the inhomogeneity of the turbulence (which is valid as $x \to 0$) and assuming r_L to be exponential. Since $T_L = T_{33}$, (15) becomes

$$\hat{K}_{33} = \overline{w'^2} T_{33}(1 - \exp(-x/L_h)), \tag{16}$$

where $L_h = \bar{u}(h)\, T_{33}(h)$, giving $L_h/h = 3.8$. This predicts that $\hat{K}_{33}/\overline{w'^2}T_{33}$, which equals the ratio of $\overline{w'\theta'}$ to term II of (14), is about 0.8 at $x/h = 7.5$ and 0.5 at $x/h = 2.5$. Figure 9 is in agreement with the prediction.

4.3. *Gradient-diffusion representations for* $\overline{u'\theta'}$

For $\overline{u'\theta'}$, (7) and (8) imply

$$\underset{\text{I}}{\overline{u'\theta'}} = \underset{\text{II}}{-\overline{u'w'} T_{13} \frac{\partial\bar{\theta}}{\partial z}} \underset{\text{III}}{- \overline{u'^2} T_{11} \frac{\partial\bar{\theta}}{\partial x}}. \tag{17}$$

Figure 10 shows the three terms of (17) at $x/h = 7.5$, 15 and 25. Terms II and III are both plotted with $T_{13} = T_{11} = \tau_\epsilon$ to show that term III is negligible, at least in

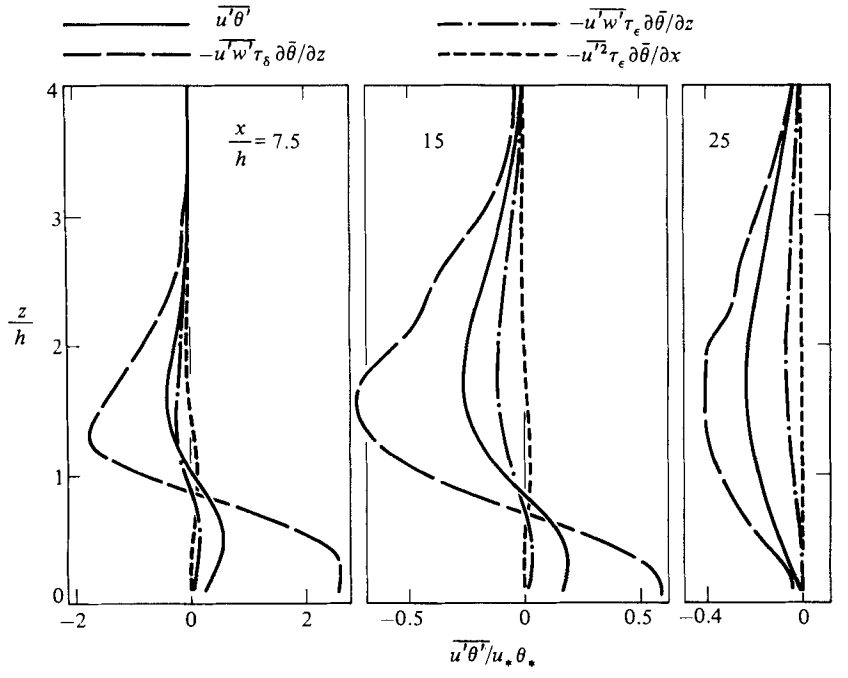

FIGURE 10. Terms in the first-order $\overline{u'\theta'}$ closure, (17).

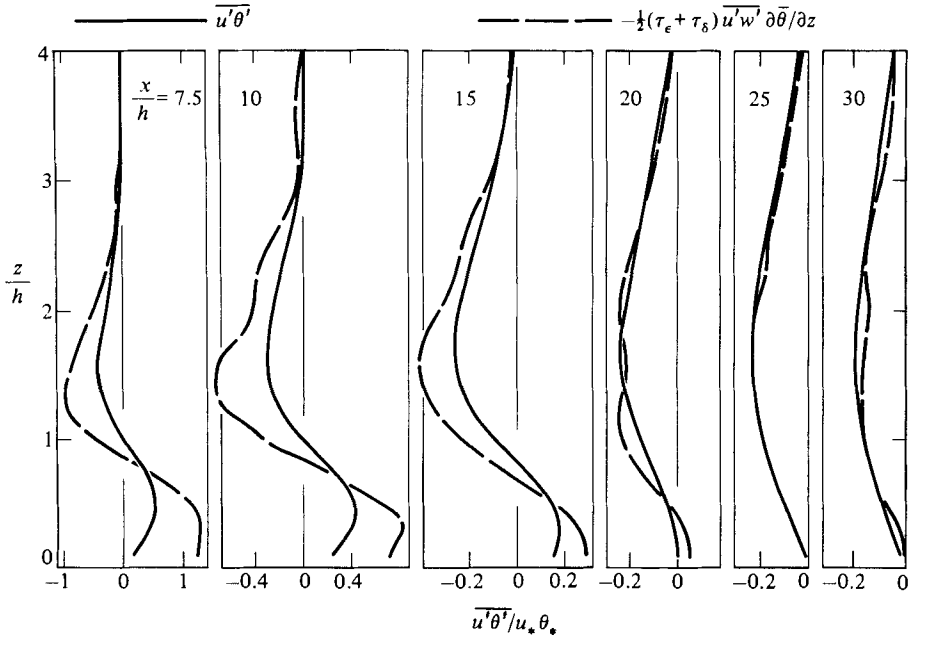

FIGURE 11. Terms in (17) (continued).

the region $x/h > 15$, where gradient-diffusion theory is valid. (The assumption $T_{31} = T_{13} = T_{11} = \tau_\epsilon$ is very poor, but suffices to show that term III is negligible in (16) and (17).) Term II is shown in figure 10 with T_{13} equal to τ_ϵ and to τ_δ, neither of which is satisfactory; $T_{13} = \tau_\delta$ gives the wrong shape with excessive predicted $\overline{u'\theta'}$ values near the ground, while $T_{13} = \tau_\epsilon$ underestimates $|\overline{u'\theta'}|$ everywhere. Since $T_{33} = \tau_\epsilon$ was successful in predicting $\overline{w'\theta'}$, it is clear that $T_{\alpha\beta}$ in (8) is not a scalar.

To find a more satisfactory value for T_{13}, we assume that T_{13} is somewhere between T_{11} and T_{33}, say their arithmetic mean. (If $T_{\alpha\beta}$ is proportional to the $u_\alpha u_\beta$ spectral peak wavelength, this assumption is consistent with spectral measurements from the atmospheric boundary layer (Kaimal 1978; Wyngaard 1980).) With $T_{33} = \tau_\epsilon$ and $T_{11} = \tau_\delta$ as before, it follows that

$$K_{13} = \tfrac{1}{2}\overline{u'w'}(\tau_\delta + \tau_\epsilon), \tag{18}$$

which is tested in figure 11 by plotting $\overline{u'\theta'}$ and $-K_{13}\partial\bar{\theta}/\partial z$ at $x/h = 7.5$, 15, 20, 25 and 30 with τ_δ fixed by (13). At the larger values of x, this crude, empirical model is successful. It fails close to the source, overpredicting $\overline{u'\theta'}$ as in the case of $\overline{w'\theta'}$; however, the region of failure for $\overline{u'\theta'}$ is larger than for $\overline{w'\theta'}$ because of the correspondingly larger timescale.

5. The budgets of temperature variance and heat flux

5.1. *The $\frac{1}{2}\overline{\theta'^2}$ budget*

The budget equation for (half the) temperature variance is, for steady, laterally homogeneous conditions,

$$\frac{\partial \frac{1}{2}\overline{\theta'^2}}{\partial t} = 0 = -\bar{u}\frac{\partial \frac{1}{2}\overline{\theta'^2}}{\partial x} - \overline{u'\theta'}\frac{\partial \bar{\theta}}{\partial x} - \overline{w'\theta'}\frac{\partial \bar{\theta}}{\partial z} - \frac{\partial}{\partial x}\frac{\overline{u'\theta'\theta'}}{2} - \frac{\partial}{\partial z}\frac{\overline{w'\theta'\theta'}}{2} - \epsilon_\theta. \tag{19}$$

The terms on the right represent advection, production by flux-gradient interactions in the streamwise and vertical directions, streamwise and vertical turbulent transport, and dissipation of temperature variance. Figure 12 shows measured values of all terms in (19) at $x/h = 7.5$, 15 and 25. The points represent directly measured values of ϵ_θ, found using (4), while the residual term is the negative sum of the measured values of the first five terms on the right of (19).

At $x/h = 7.5$, the budget of $\frac{1}{2}\overline{\theta'^2}$ is basically a balance between advection (gain) and dissipation (loss) in the plume core, and between upward turbulent transport (gain) and advection (loss) in the upper wing. Close to the ground, the balance is essentially between downward turbulent transport (gain) and dissipation (loss). There is relatively little local production, almost all the $\frac{1}{2}\overline{\theta'^2}$ being advected from upstream, whence it originates in strong production zones very close to the source itself. The amount of $\frac{1}{2}\overline{\theta'^2}$ produced in these zones, and hence the variance field and budget, depends on source size (see FR and §3.2). With increasing x, the terms change in relative importance. At the largest available fetch ($x/h = 25$), vertical production is just as important a gain term in the plume core as advection, while vertical turbulent transport is more important, compared with the situation at smaller x, as a loss near the plume core. Not surprisingly, streamwise production and transport are negligible at all values of x.

The agreement between direct and residual measurements of ϵ_θ is satisfactory. In assessing these results, one must take into account not only the experimental

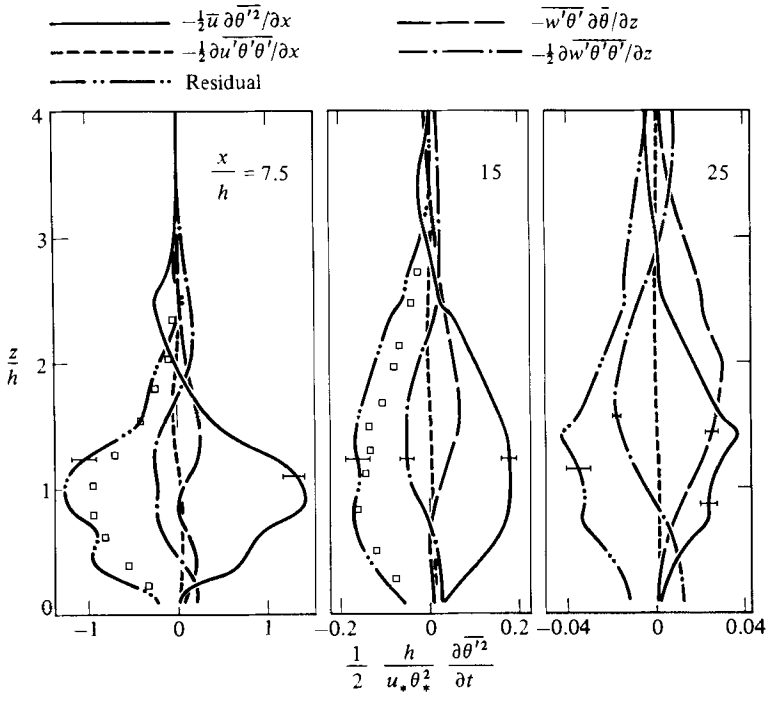

FIGURE 12. Terms in the budget of $\frac{1}{2}\overline{\theta'^2}$, (19). Error bars as in figure 8. □: direct measurements of ϵ_θ. Streamwise production (not plotted) is negligible.

uncertainties (which are likely to be no larger than those in the $\bar{\theta}$-budget, figure 8) but also the fact that the direct method assumes Taylor's hypothesis and the local-isotropy consequence $\overline{\theta_x'^2} = \overline{\theta_y'^2} = \overline{\theta_z'^2}$ (subscripts denoting differentiation). Like Bradley, Antonia & Chambers (1981), we apply no correction for the known deficiencies of Taylor's hypothesis at even moderate turbulence intensities. The assumption $\overline{\theta_x'^2} = \overline{\theta_y'^2} = \overline{\theta_z'^2}$ has been contradicted by the direct measurements of Sreenivasan *et al.* (1977) in a turbulent boundary layer with a slightly heated wall, in which they found $\overline{\theta_x'^2}:\overline{\theta_y'^2}:\overline{\theta_z'^2}$ to be approximately 1.0:1.4:1.2. This result, if general, would imply that (4) underestimates ϵ_θ by about 20%. The ϵ_θ measurements in figure 12 are consistent with such an underestimate.

In comparing our $\frac{1}{2}\overline{\theta'^2}$ budgets with those of FR for an elevated point source, we observe broad similarity apart from the relative importance of the production and transport terms. Within each experiment, production and transport were comparable (except for FR's budget at $x/h = 10$, which was anomalous). However, FR found that production and transport remained much smaller than advection and dissipation, even at $x/h = 30$; in contrast, production is just as large as advection for our line source at $x/h = 25$, and presumably becomes larger with further increase in x. The difference is not related to source size ($d/h = 0.015$ in our case and 0.039 for FR), but rather to the same distinction between point and line sources as was evident for σ_θ (§3.2).

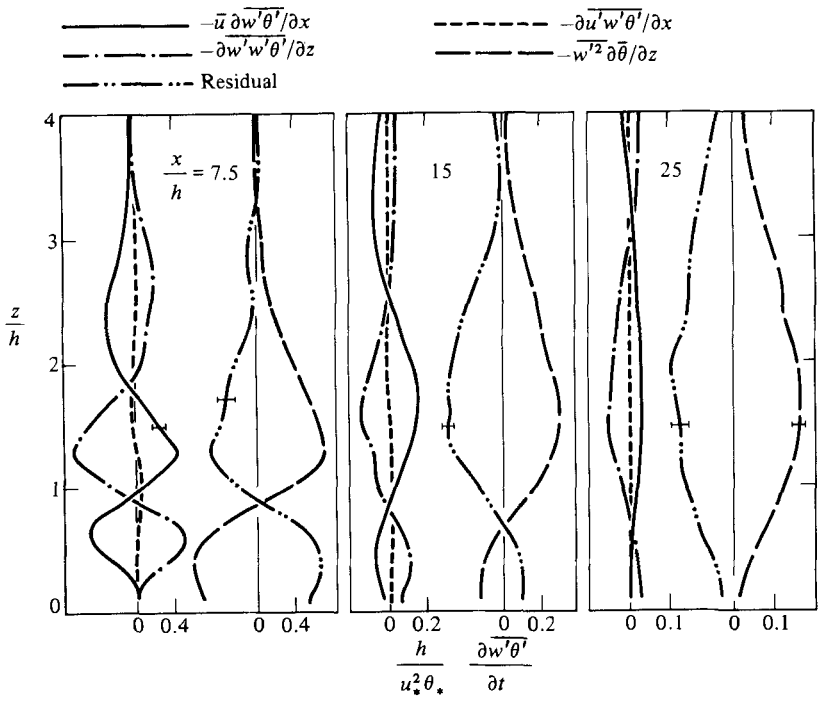

FIGURE 13. Terms in the budget of $\overline{w'\theta'}$, (20). Error bars as in figure 8. Streamwise production (not plotted) is negligible.

5.2. *The $\overline{w'\theta'}$ budget*

The vertical heat-flux budget is, in steady, laterally homogeneous conditions,

$$\frac{\partial\overline{w'\theta'}}{\partial t} = 0 = -\bar{u}\frac{\partial\overline{w'\theta'}}{\partial x} - \overline{u'w'}\frac{\partial\bar{\theta}}{\partial x} - \overline{w'^2}\frac{\partial\bar{\theta}}{\partial z} - \frac{\partial}{\partial x}\overline{u'w'\theta'} - \frac{\partial}{\partial z}\overline{w'w'\theta'}$$

$$- \overline{\theta'\frac{\partial p'}{\partial z}} + \nu\overline{\theta'\nabla^2 w'} + \kappa\overline{w'\nabla^2\theta'}. \quad (20)$$

The molecular terms vanish with the assumption of local isotropy and will be neglected here. The first five terms on the right-hand side (representing advection, production and turbulent transport) were directly measured and are shown in figure 13 for $x/h = 7.5$, 15 and 25. Also shown is the residual (the negative sum of the directly measured terms), which is a measurement by difference of the pressure term plus the negligible molecular terms. Unlike the $\frac{1}{2}\overline{\theta'^2}$ budget, neither the $\overline{w'\theta'}$ nor the $\overline{u'\theta'}$ budget is significantly dependent on source size.

The striking feature of the $\overline{w'\theta'}$ budget is the near-perfect balance between advection and (vertical) transport. Advection acts as a gain near the plume core and a loss in the wings (at least until the lower wing hits the ground at $x/h \approx 25$), while transport acts in the reverse way. Similar behaviour was observed by FR on the centreline of plumes from elevated point sources. Since streamwise transport and production are negligible, the implication of this balance is that vertical production of $\overline{w'\theta'}$ is in local equilibrium with the pressure-gradient interaction term, which 'destroys' $\overline{w'\theta'}$. This is discussed further in §6.1.

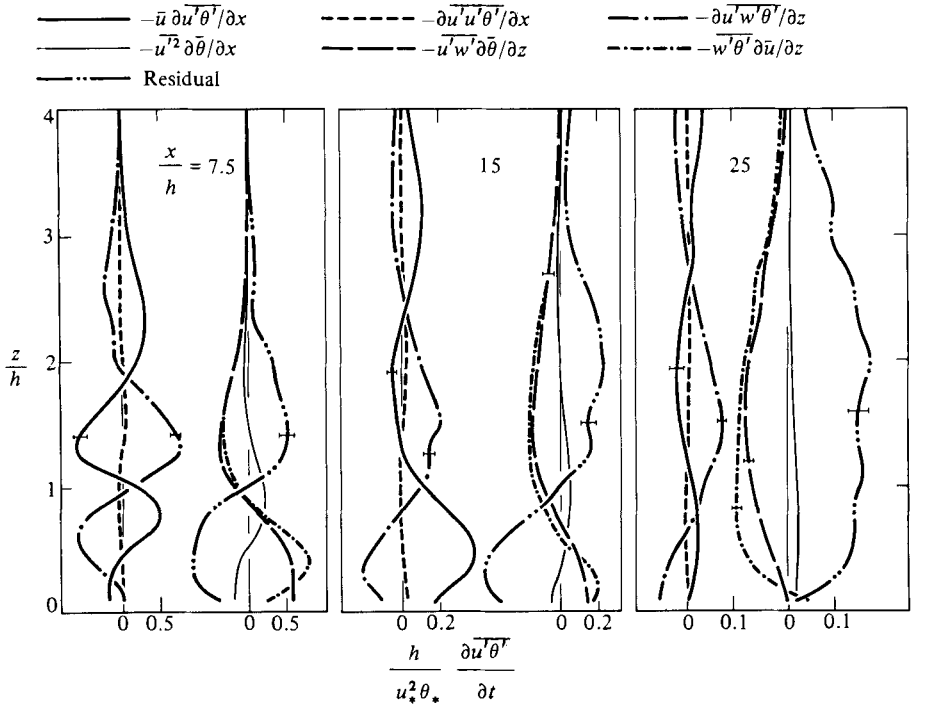

FIGURE 14. Terms in the budget of $\overline{u'\theta'}$, (21). Error bars as in figure 8.

5.3. *The $\overline{u'\theta'}$ budget*

The streamwise heat-flux budget is, in steady, laterally homogeneous conditions,

$$\frac{\partial\overline{u'\theta'}}{\partial t} = 0 = -\bar{u}\frac{\partial\overline{u'\theta'}}{\partial x} - \overline{u'\theta'}\frac{\partial\bar{u}}{\partial x} - \overline{w'\theta'}\frac{\partial\bar{u}}{\partial z} - \overline{u'^2}\frac{\partial\bar{\theta}}{\partial x} - \overline{u'w'}\frac{\partial\bar{\theta}}{\partial z} - \frac{\partial}{\partial x}\overline{u'u'\theta'} - \frac{\partial}{\partial z}\overline{u'w'\theta'}$$
$$-\overline{\theta'\frac{\partial p'}{\partial x}} + \nu\overline{\theta'\nabla^2 u'} + \kappa\overline{u'\nabla^2\theta'}, \quad (21)$$

which includes advection, four production terms (from wind and temperature gradients in the streamwise and vertical directions), two transport terms, a pressure-gradient interaction term and molecular terms. As for the $\overline{w'\theta'}$ budget, we dismiss the molecular terms as negligible; Bradley, Antonia & Chambers (1982) have shown by measurement in the atmospheric surface layer that these terms are small in the $\overline{u'\theta'}$ budget. Figure 14 shows measurements at $x/h = 7.5$, 15 and 25 of the other terms in (21), including a residual measurement of the pressure term but excepting $-\overline{u'\theta'}\,\partial\bar{u}/\partial x$, which effectively vanishes because $\partial\bar{u}/\partial x \approx 0$.

In this budget, streamwise transport is negligible but production from $\partial\bar{\theta}/\partial x$ is not, so three significant production terms must be considered. The balance between advection and vertical transport, so conspicuous for the $\overline{w'\theta'}$ budget, is here only approximate. No comparison can be made with FR as they did not present $\overline{u'\theta'}$ budgets. One interesting feature is that the ratio between the vertical production terms $\overline{u'w'}\,\partial\bar{\theta}/\partial z$ and $\overline{w'\theta'}\,\partial\bar{u}/\partial z$ is the turbulent Prandtl number Pr, which is close to the expected surface-layer value of unity except near the surface ($z/h < 1$), where it is substantially less than 1. This feature has also been observed in the atmosphere (Raupach & Thom 1981).

6. Tests of second-order closure models

6.1. *Pressure terms in the $\overline{u_i'\theta'}$ equation*

This section compares measurements of pressure, transport and dissipation terms in the $\overline{u_i'\theta'}$ and $\frac{1}{2}\overline{\theta'^2}$ budgets with models for these terms which are commonly used in single-point, second-order-closure schemes for calculating scalar transport in turbulent flows.

The pressure term in the $\overline{u_i'\theta'}$ budget is usually modelled by first expressing p', via its Poisson equation, as the sum of integrals over the entire flow of nonlinear (turbulence-interaction) and linear (rapid) terms which are functions of the fluctuating velocities, and then approximating each integral by a single-point quantity (Launder 1976; Lumley 1978; Zeman 1981). The most common model of this type is

$$\phi_{i\theta} = -\overline{\theta'\frac{\partial p'}{\partial x_i}} = \phi_{i\theta 1} + \phi_{i\theta 2} + \phi_{i\theta 3}, \tag{22}$$

$$\phi_{i\theta 1} = -\overline{u_i'\theta'}/\tau, \tag{23}$$

$$\phi_{i\theta 2} = \tfrac{4}{5}\overline{u_j'\theta'}\frac{\partial \bar{u}_i}{\partial x_j} - \tfrac{1}{5}\overline{u_j'\theta'}\frac{\partial \bar{u}_j}{\partial x_i}, \tag{24}$$

$$\phi_{i\theta 3} = \frac{1}{3}\frac{g_i}{T_a}\overline{\theta'^2}, \tag{25}$$

where $\phi_{i\theta 1}$ is the turbulence-interaction contribution to $\phi_{i\theta}$, $\phi_{i\theta 2}$ the mean-strain contribution and $\phi_{i\theta 3}$ the buoyancy contribution, the last two being the rapid terms; $g_i = (0, 0, -g)$ is the gravitational acceleration vector, and τ a timescale which is usually taken to be τ_ϵ (see, for example, the above three references). This model is not universally accepted, and has some unphysical properties (Wyngaard 1980, 1981). Nevertheless, as a preliminary closure investigation, we test (23) and (24) here. In our non-buoyant flow, (25) vanishes.

Gibson & Launder (1978) discuss 'surface additions' to (23)–(25), intended to account for the fact that the solution to the Poisson equation for p' involves an integral over the bounding surface as well as a volume integral over the flow. For our plane surface-layer flow, their proposed surface additions to $\phi_{i\theta 2}$ and $\phi_{i\theta 3}$ both vanish and that for $\phi_{i\theta 1}$ has no effect except to change τ (by a proportionality constant) from the value it would adopt in free shear flows.

We first consider the pressure term in the $\overline{w'\theta'}$ equation. For our geometry, (22)–(24) give

$$\underset{\text{I}}{-\overline{\theta'\frac{\partial p'}{\partial z}}} = \underset{\text{II}}{-\frac{\overline{w'\theta'}}{\tau}} \underset{\text{III}}{-\tfrac{1}{5}\overline{u'\theta'}\frac{\partial \bar{u}}{\partial z}}. \tag{26}$$

Figure 15 shows terms I, II and III of (26) at $x/h = 7.5$, 15 and 25, with $\tau = \tau_\epsilon$. The value $c_\epsilon = 0.09$, used in first-order closure tests, was retained. The sum II + III provides a satisfactory model of term I except, possibly, near the ground ($z/h < 0.5$). The mean-strain contribution, term III, is largest near the ground but seems to improve the model overall.

For the pressure term in the $\overline{u'\theta'}$ equation, (22)–(24) imply, with our geometry,

$$\underset{\text{I}}{-\overline{\theta'\frac{\partial p'}{\partial x}}} = \underset{\text{II}}{-\frac{\overline{u'\theta'}}{\tau}} \underset{\text{III}}{+\tfrac{4}{5}\overline{w'\theta'}\frac{\partial \bar{u}}{\partial z}}, \tag{27}$$

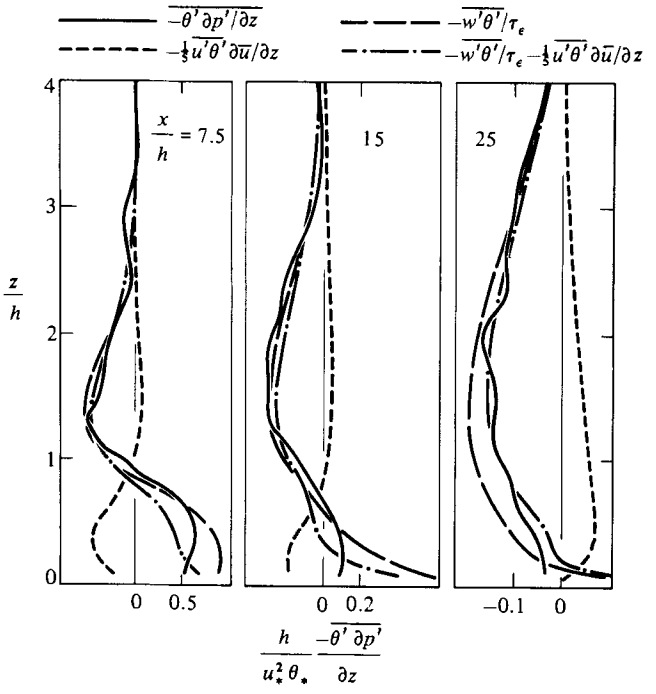

FIGURE 15. Terms in the closure for $-\overline{\theta'\partial p'/\partial z}$, (26).

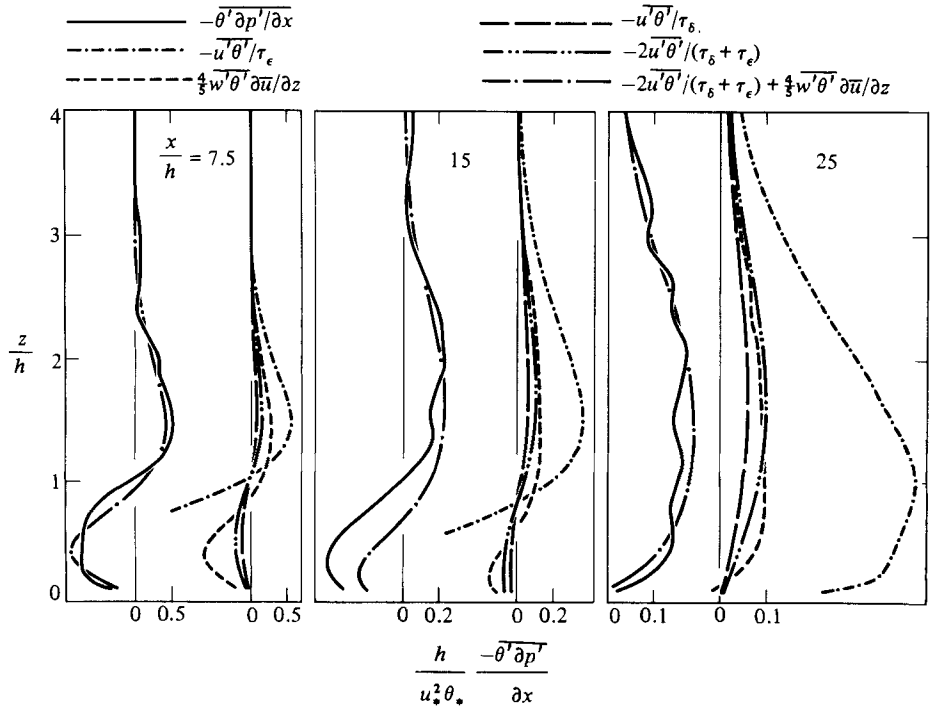

FIGURE 16. Terms in the closure for $-\overline{\theta'\partial p'/\partial z}$, (27).

in which the various terms are shown for $x/h = 7.5$, 15 and 25 in figure 16. Unlike (26), the mean-strain term III in (27) is a substantial fraction of term I. If τ is set equal to τ_ϵ (the conventional value, which was satisfactory in (26)), then the turbulence-interaction term, II, is grossly wrong in (27), especially near the ground. The choice $\tau = \frac{1}{2}(\tau_\delta + \tau_\epsilon)$ (the value given to T_{13} in the gradient-diffusion model for $\overline{u'\theta'}$) produces a model (II + III) of term I which is broadly satisfactory, although there remain significant errors of detail such as the zero-crossing height at $x/h = 15$. However, by using different values for τ in the models (26) and (27), we have violated the requirement that τ in (23) be a scalar. The conclusion is that (23), with a scalar τ, is not a satisfactory model of the turbulence-interaction term.

This is consistent with the conclusion for $T_{\alpha\beta}$, the timescale in the gradient-diffusion model for $\overline{u_i'\theta'}$, as we show by examining the restricted circumstances under which the $\overline{u_i'\theta'}$ equation reduces to a gradient-diffusion equation. For a steady non-buoyant flow in which advection and turbulent transport are negligible or are in balance, the $\overline{u_i'\theta'}$ equation is (neglecting molecular terms)

$$0 = -\overline{u_i'u_j'}\frac{\partial\bar{\theta}}{\partial x_j} - \overline{u_j'\theta'}\frac{\partial\bar{u}_i}{\partial x_j} + \phi_{i\theta}. \tag{28}$$

Assume that $\phi_{i\theta}$ can be modelled as the sum of a turbulent-interaction term (23) and a mean-strain term which cancels the whole of the production term $-\overline{u_j'\theta'}\,\partial\bar{u}_i/\partial x_j$ in (28), not just most of it as does the model (24) for the mean-strain term. Then (28) reduces to

$$0 = -\overline{u_i'u_j'}\frac{\partial\bar{\theta}}{\partial x_j} - \frac{\overline{u_i'\theta'}}{\tau}, \tag{29}$$

which is identical with the gradient-diffusion model (7) and (8) if τ is identified with $T_{\alpha\beta}$. These restrictions and idealizations hold fairly closely in our experiment; in particular, advection and turbulent transport of $\overline{u_i'\theta'}$ are in approximate balance. Hence, the non-scalar nature of $T_{\alpha\beta}$ in the gradient-diffusion model is directly linked with the failure of (23) with a scalar τ. This failure is the reason that second-order closure models using (23), with a scalar τ, encounter major difficulties in predicting $\overline{u'\theta'}$ (Launder 1976; Zeman & Lumley 1979). Large adjustments of numerical coefficients are required to enable such models to predict $\overline{u'\theta'}$ satisfactorily.

6.2. *Transport terms in the $\frac{1}{2}\overline{\theta'^2}$ and $\overline{u_i'\theta'}$ equations*

The triple products appearing in the transport terms are usually modelled with the gradient-diffusion assumptions

$$\overline{u_i'\theta'^2} = -\tau\overline{u_i'u_j'}\frac{\partial\overline{\theta'^2}}{\partial x_j}, \tag{30}$$

$$\overline{u_i'u_j'\theta'} = -\tau\overline{u_i'u_k'}\frac{\partial\overline{u_j'\theta'}}{\partial x_k} - \tau\overline{u_j'u_k'}\frac{\partial\overline{u_i'\theta'}}{\partial x_k}, \tag{31}$$

where τ is a scalar timescale (Launder 1976; Lumley 1978). According to (30) and (31), the dominant (vertical) transport terms in the $\frac{1}{2}\overline{\theta'^2}$, $\overline{w'\theta'}$ and $\overline{u'\theta'}$ budgets can be modelled using

$$\tfrac{1}{2}\overline{w'\theta'^2} = -\tau\overline{w'^2}\frac{\partial\frac{1}{2}\overline{\theta'^2}}{\partial z}, \tag{32}$$

$$\overline{w'w'\theta'} = -2\tau\overline{w'^2}\frac{\partial\overline{w'\theta'}}{\partial z}, \tag{33}$$

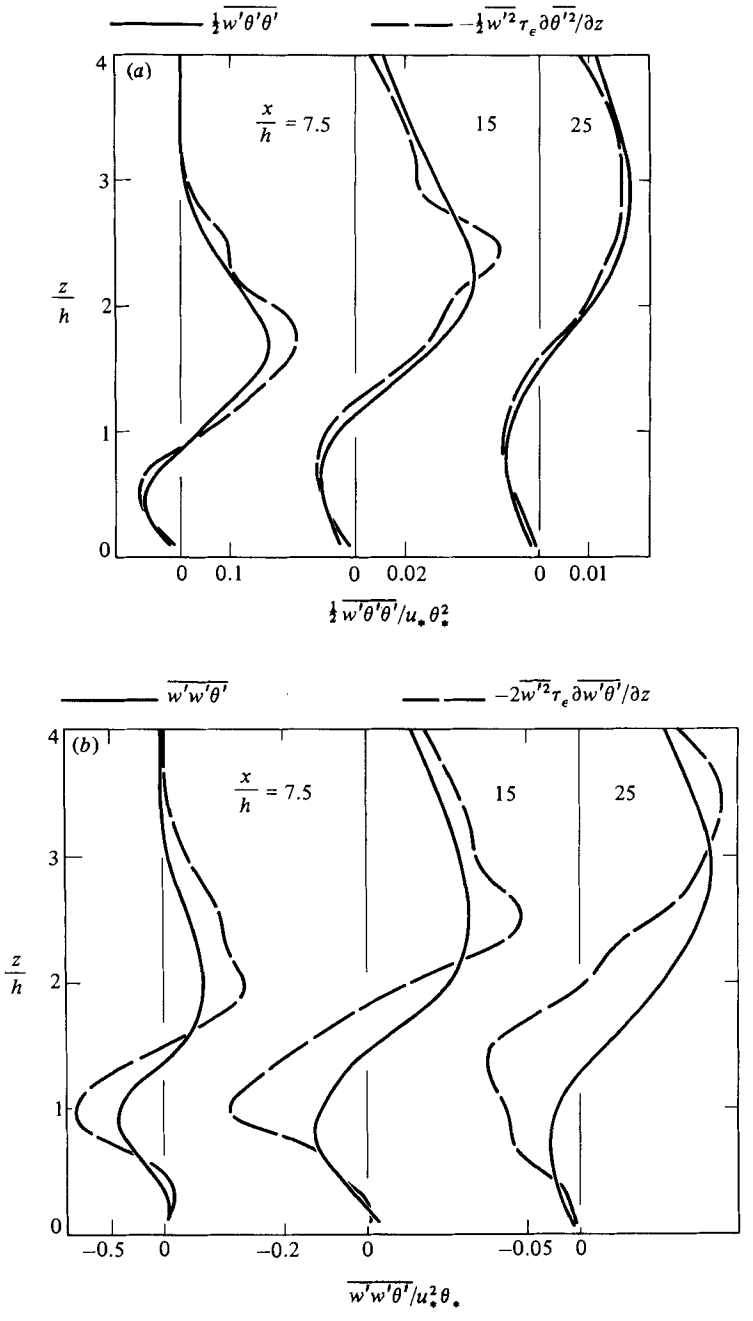

FIGURE 17 (*a*, *b*). For caption see p. 134.

$$\overline{u'w'\theta'} = -\tau\overline{u'w'}\frac{\partial\overline{w'\theta'}}{\partial z} - \tau\overline{w'^2}\frac{\partial\overline{u'\theta'}}{\partial z}. \tag{34}$$

Terms in streamwise gradients have been ignored because they are negligible. Tests of (32)–(34) are shown in figure 17, with τ taken as τ_ϵ. The model (32) for $\frac{1}{2}\overline{w'\theta'^2}$ is adequate, but for $\overline{w'w'\theta'}$ and $\overline{u'w'\theta'}$, significant shape differences are evident between

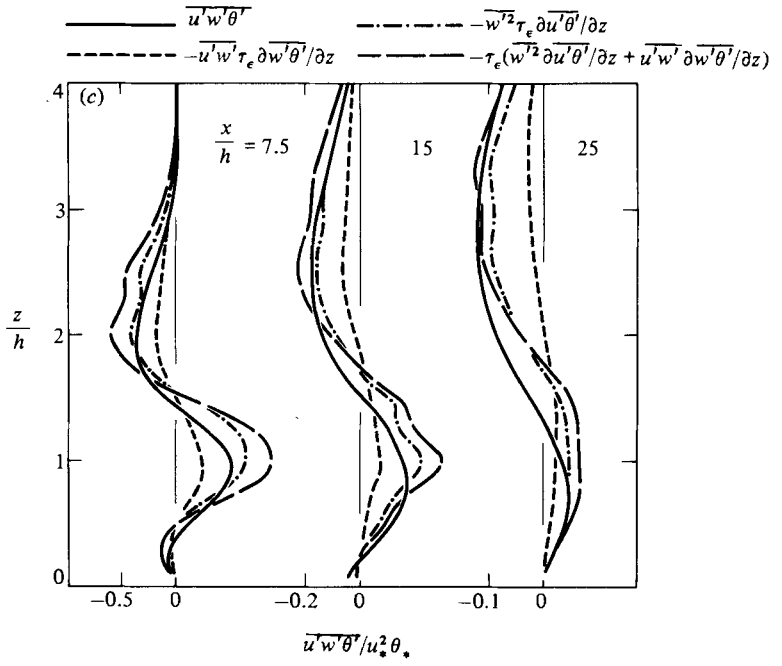

FIGURE 17. (*a*) Terms in the $\frac{1}{2}\overline{w'\theta'^2}$ closure, (32). (*b*) Terms in the $\overline{w'^2\theta'}$ closure, (33). (*c*) Terms in the $\overline{u'w'\theta'}$ closure, (34).

the triple moments and their models; in particular, the zero-crossing heights are seriously wrong at $x = 1.50$ m. This situation cannot be improved by a different choice of timescale.

Note that the transport timescale τ in (30)–(34) needs modification close to the source in the same way as the effective diffusivity $\hat{K}$ in (15) and (16); however, the timescale for the turbulence-interaction component of the pressure term, in (23) *et seq.*, does not need this modification (Deardorff 1978).

6.3. *The dissipation rate for temperature variance*

The temperature dissipation rate ϵ_θ is sometimes modelled using its own rate equation, but crude models for ϵ_θ do exist. The simplest, applicable only when the velocity and temperature fields are both in local equilibrium, is that the dissipative timescales $\overline{q^2}/2\epsilon$ for $\frac{1}{2}\overline{q^2}$ and $\overline{\theta'^2}/2\epsilon_\theta$ for $\frac{1}{2}\overline{\theta'^2}$ are proportional with ratio R; R is 1 in decaying grid turbulence (Warhaft & Lumley 1978) and about 0.5 in the near-neutral atmospheric surface layer (Antonia, Chambers & Bradley 1981). It follows that

$$\epsilon_\theta = \frac{c_\epsilon R \frac{1}{2}\overline{\theta'^2}}{\tau_\epsilon}, \tag{35}$$

which is tested in figure 18 by plotting both sides of (35) with $R = 1$ and c_ϵ as before. The hypothesis is quite incorrect, which is not surprising given that the $\frac{1}{2}\overline{\theta'^2}$ budget is far from local equilibrium.

A second model for ϵ_θ was suggested by FR to describe dispersion from point sources in a turbulent boundary layer:

$$\epsilon_\theta = \frac{\frac{1}{2}\overline{\theta'^2}}{c_\theta \sigma_z/\sigma_q}, \tag{36}$$

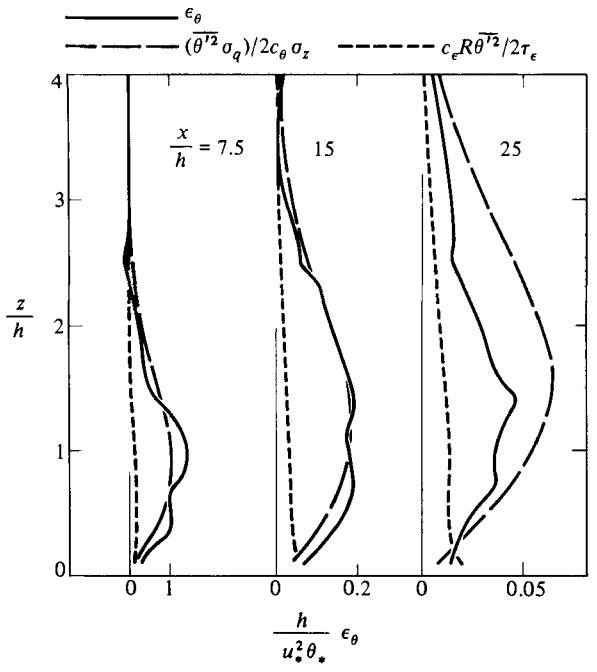

FIGURE 18. The ϵ_θ closure.

where c_θ is a constant, $\sigma_z(x)$ the plume depth (defined so that $\sigma_z^2(x)$ is the centred second moment of $\bar{\theta}(x,z)$ along a vertical slice through the plume at x) and where $\sigma_q = (\frac{1}{2}\overline{q^2})^{\frac{1}{2}}$. Here the dissipative timescale for $\frac{1}{2}\overline{\theta'^2}$ is $c_\theta\sigma_z/\sigma_q$, which is not strongly z-dependent (unlike τ_ϵ) but which grows with x, like σ_z. Equation (36) is also tested in figure 18, with $c_\theta = 2.0$ (a value chosen to optimize (36) at $x/h = 15$). Its performance is fair only. If (36) defines c_θ, then c_θ increases with x from less than 2 at $x/h = 7.5$ to more than 3 at $x/h = 25$. These values fall within the considerable scatter of FR's data.

7. Conclusions

The conclusions of this work may be summarized as follows.

(1) Tests of first-order closure have shown that a gradient-diffusion theory predicts $\overline{w'\theta'}$ and $\overline{u'\theta'}$ quite well in this flow, except close to the source ($x/h \lesssim 1$). The gradient-diffusion prediction for $\overline{u'\theta'}$ is dominated by the off-diagonal component K_{13} of the diffusivity tensor. To use gradient-diffusion theory successfully, it is essential to account for the existence of multiple timescales in the boundary layer by using different timescales for the different elements of $K_{\alpha\beta} = \overline{u'_\alpha u'_\beta}\,T_{\alpha\beta}$. Suitable scales were found to be τ_ϵ for K_{33} and $\frac{1}{2}(\tau_\delta + \tau_\epsilon)$ for K_{13}, the latter scale being no more than an empirical one which fits the present data.

(2) The budget of $\frac{1}{2}\overline{\theta'^2}$ is dominated by advection (gain) and dissipation (loss), except at large x, where production becomes significant. Direct measurements of ϵ_θ, from the variance of $\partial\theta'/\partial t$ with assumptions of local isotropy and Taylor's hypothesis, are about 20 % lower than ϵ_θ values from the $\frac{1}{2}\overline{\theta'^2}$ budget residual. This is consistent with a failure of local isotropy such that $\overline{\theta'^2_x} < (\overline{\theta'^2_y}, \overline{\theta'^2_z})$.

(3) The $w'\theta'$ budget is close to local equilibrium in the sense that the advection and vertical transport terms cancel, leaving only a balance between vertical

production and pressure terms. The pressure term is dominated by a turbulence-interaction component which can be successfully modelled as $-\overline{w'\theta'}/\tau$, where $\tau = \tau_\epsilon$ is the same timescale as that appearing in the first-order diffusivity K_{33}.

(4) The $\overline{u'\theta'}$ budget is more complicated than the $\overline{w'\theta'}$ budget, because the advection and turbulent transport terms are only approximately self-cancelling and because there are three significant production terms, including one from the streamwise temperature gradient. Accordingly, the experimental conclusions are less precise. What is certain is that the turbulence-interaction component of the pressure term in the $\overline{u'\theta'}$ budget, $-\overline{u'\theta'}/\tau$, must use a timescale different from that in the corresponding term in the $\overline{w'\theta'}$ budget. The choice $\tau = \frac{1}{2}(\tau_\delta + \tau_\epsilon)$, the same timescale as found to work in the first-order diffusivity $K_{13} = \overline{u'w'}T_{13}$, is satisfactory. The mean-strain component is also significant in the pressure term in the $\overline{u'\theta'}$ equation.

(5) Because the turbulence-interaction component of the pressure term requires different timescales in the $\overline{u'\theta'}$ and $\overline{w'\theta'}$ equations, the model $\phi_{i1} = \overline{u_i'\theta'}/\tau$ (where τ is necessarily scalar) is not adequate.

(6) The triple products in the turbulent transport terms are not well represented by gradient-diffusion models, except for the product $\frac{1}{2}\overline{w'\theta'^2}$ in the $\frac{1}{2}\overline{\theta'^2}$ equation.

(7) In comparing these data (line source with $h/\delta = 0.11$) with those of FR (point source with $h/\delta = 0.19$, in an essentially identical boundary layer) two main points emerge: firstly, the $\bar{\theta}$ and $\overline{w'\theta'}$ fields are similar under surface-layer scaling (lengths scaled with h). Consequently, the flux budgets are likewise similar. Secondly, the σ_θ fields are not similar, the relative intensity $\sigma_\theta/\bar{\theta}$ being much smaller for the line than for the point source. This is consistent with the known dependence of $\sigma_\theta/\bar{\theta}$ on source size. Likewise, the $\frac{1}{2}\overline{\theta'^2}$ budgets are dissimilar, with local production (apart from the strong production zones very close to the source itself) being even less important for the point source than for the line source.

REFERENCES

ANTONIA, R. A., CHAMBERS, A. J. & BRADLEY, E. F. 1981 Temperature structure in the atmospheric surface layer II. The budget of mean cube fluctuations. *Boundary-Layer Met.* **20**, 293–307.

BATCHELOR, G. K. 1949 Diffusion in a field of homogeneous turbulence. I. Eulerian analysis. *Austral. J. Sci. Res.* **2**, 437–450.

BATCHELOR, G. K. 1957 Diffusion in free turbulent shear flows. *J. Fluid Mech.* **3**, 67–80.

BELORGEY, M., NGUYEN, A. D. & TRINITE, M. 1980 Diffusion from a line source in a turbulent boundary layer with transfer to the wall. In *Turbulent Shear Flows 2* (ed. L. J. S. Bradbury, F. Durst, B. E. Launder, F. W. Schmidt & J. H. Whitelaw), pp. 129–142. Springer.

BRADLEY, E. F., ANTONIA, R. A. & CHAMBERS, A. J. 1981 Temperature structure in the atmospheric surface layer. I. The budget of temperature variance. *Boundary-Layer Met.* **20**, 275–292.

BRADLEY, E. F., ANTONIA, R. A. & CHAMBERS, A. J. 1982 Streamwise heat flux budget in the atmospheric surface layer. *Boundary-Layer Met.* **23**, 3–15.

CHAMPAGNE, F. H., SLEICHER, C. A. & WEHRMANN, O. H. 1967 Turbulence measurements with inclined hot wires. Part 1. Heat transfer experiments with inclined hot-wire. *J. Fluid Mech.* **28**, 153–175.

COLLIS, D. C. & WILLIAMS, M. J. 1959 Two-dimensional convection from heated wires at low Reynolds numbers. *J. Fluid Mech.* **6**, 357–384.

CORRSIN, S. 1974 Limitations of gradient-transport models in random walks and in turbulence. *Adv. Geophys.* **18A**, 25–60.

DEARDORFF, J. W. 1978 Closure of second- and third-moment rate equations for diffusion in homogeneous turbulence. *Phys. Fluids* **21**, 525–530.

DE BOOR, C. 1978 *A Practical Guide to Splines*. Springer.

FACKRELL, J. E. & ROBINS, A. G. 1981 Passive emissions from point sources in turbulent boundary layers. In *Proc. 3rd Symp. on Turbulent Shear Flows, September* 1981, pp. 9.7–9.12. University of California at Davis.

FACKRELL, J. E. & ROBINS, A. G. 1982 Concentration fluctuations and fluxes in plumes from point sources in a turbulent boundary layer. *J. Fluid Mech.* **117**, 1–26.

GIBSON, M. M. & LAUNDER, B. E. 1978 Ground effects on pressure fluctuations in the atmospheric surface layer. *J. Fluid Mech.* **86**, 491–511.

HUNT, J. C. R. & WEBER, A. H. 1979 A Lagrangian statistical analysis of diffusion from a ground-level source in a turbulent boundary layer. *Q. J. R. Met. Soc.* **105**, 423–443.

KAIMAL, J. C. 1978 Horizontal velocity spectra in an unstable surface layer. *J. Atmos. Sci.* **35**, 18–24.

LAUNDER, B. E. 1976 Heat and mass transport. In *Turbulence* (ed. P. Bradshaw). Springer.

LEGG, B. J. 1983 Turbulent diffusion from an elevated line source: Markov chain simulations of concentration and flux profiles. *Q. J. R. Met. Soc.* **109**, 645–660.

LUMLEY, J. 1978 Computational modeling of turbulent flows. *Adv. Appl. Mech.* **18**, 124–176.

MONIN, A. S. & YAGLOM, A. M. 1971 *Statistical Fluid Mechanics*, vol. 1. MIT Press.

MULHEARN, P. J. & FINNIGAN, J. J. 1978 Turbulent flow over a very rough, random surface. *Boundary-Layer Met.* **15**, 109–132.

RAUPACH, M. R. 1981 Conditional statistics of Reynolds stress in rough-wall and smooth-wall turbulent boundary layers. *J. Fluid Mech.* **108**, 363–382.

RAUPACH, M. R. & THOM, A. S. 1981 Turbulence in and above plant canopies. *Ann. Rev. Fluid Mech.* **13**, 97–129.

RAUPACH, M. R., THOM, A. S. & EDWARDS, I. 1980 A wind tunnel study of turbulent flow close to regularly arrayed rough surfaces. *Boundary-Layer Met.* **18**, 373–397.

ROBINS, A. G. & FACKRELL, J. E. 1979 Continuous plumes – their structure and prediction. In *Mathematical Modelling of Turbulent Diffusion in the Environment* (ed. C. J. Harris), pp. 55–114. Academic.

SHLIEN, P. J. & CORRSIN, S. 1976 Dispersion measurements in a turbulent boundary layer. *Intl J. Heat and Mass Transfer* **19**, 285–295.

SREENIVASAN, K. R., ANTONIA, R. A. & DANH, H. Q. 1977 Temperature dissipation fluctuations in a turbulent boundary layer. *Phys. Fluids* **20**, 1238–1249.

SUTTON, O. G. 1953 *Micrometeorology*. McGraw-Hill.

WARHAFT, Z. & LUMLEY, J. L. 1978 An experimental study of the decay of temperature fluctuations in grid-generated turbulence. *J. Fluid Mech.* **88**, 659–684.

WOODING, R. A. 1968 A low-speed wind tunnel for model studies in micrometeorology. *Austral. CSIRO Div. Plant Ind. Tech. Paper* 25.

WYNGAARD, J. C. 1980 The atmospheric boundary layer – modeling and measurements. In *Turbulent Shear Flows 2* (ed. L. J. S. Bradbury, F. Durst, B. E. Launder, F. W. Schmidt & J. H. Whitelaw), pp. 352–365. Springer.

WYNGAARD, J. C. 1981 Boundary-layer modeling. In *Atmospheric Turbulence and Air Pollution Modelling* (ed. F. T. M. Nieuwstadt & H. van Dop), pp. 69–106. Reidel.

ZEMAN, O. 1981 Progress in the modeling of planetary boundary layers. *Ann. Rev. Fluid Mech.* **13**, 253–272.

ZEMAN, O. & LUMLEY, J. L. 1979 Buoyancy effects in entraining turbulent boundary layers: a second-order closure study. In *Turbulent Shear Flows I* (ed. F. Durst, B. E. Launder, F. W. Schmidt & J. H. Whitelaw), pp. 295–306. Springer.